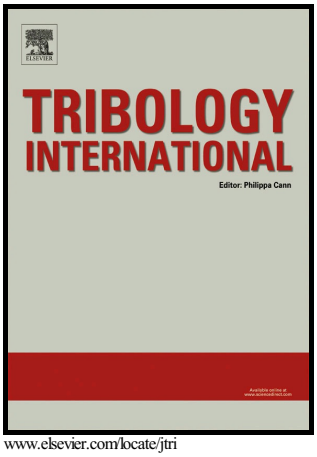

www.elsevier.com/locate/jtri

Higher in-flight particle velocities enhance in vitro tribological behavior of plasma sprayed hydroxyapatite coatings

N.W. Khun, Z. Li, K.A. Khor, J. Cizek

PII: S0301-679X(16)30252-3
DOI: http://dx.doi.org/10.1016/j.triboint.2016.08.006
Reference: JTRI4312

To appear in: *Tribiology International*

Received date: 8 March 2016
Revised date: 27 July 2016
Accepted date: 5 August 2016

Cite this article as: N.W. Khun, Z. Li, K.A. Khor and J. Cizek, Higher in-fligh particle velocities enhance in vitro tribological behavior of plasma sprayed hydroxyapatite coatings, *Tribiology International* http://dx.doi.org/10.1016/j.triboint.2016.08.006

Higher in-flight particle velocities enhance in vitro tribological behavior of plasma sprayed hydroxyapatite coatings

N. W. Khun[a], Z. Li[a], K. A. Khor[a], J. Cizek[b,*]

[a] School of Mechanical and Aerospace Engineering, Nanyang Technological University, 50 Nanyang Avenue, 639798, Singapore

[b] Netme Centre, Institute of Materials Science and Engineering, Brno University of Technology, Technicka 2896/2, 61669 Brno, Czech Republic

* Corresponding author: cizek@fme.vutbr.cz, Tel: +420 541 143 166

Abstract

Hydroxyapatite (HA) coatings were deposited onto Ti6Al4V substrates via atmospheric plasma spraying under systematically varying spray parameters, leading to different in-flight particle velocities. Morphology, composition, and tribological properties of the coatings were then studied. The coatings deposited at higher in-flight particle velocities exhibited smoother surface topography, better inter-particle bonding and higher Young's modulus and hardness. Ball-on-disc tribological results showed that the friction and wear of the HA coatings significantly decreased with increased in-flight particle velocity in both dry and wet (Hanks' solution) conditions. All HA coatings exhibited lower friction and wear during the wet sliding due to the lubricating effect of the solution.

Keywords: HA coating; thermal spraying; bio-tribology; Hanks' solution; friction; wear

1. Introduction

As one of the most widely used bioceramics, hydroxyapatite (HA) has been traditionally utilized in orthopedic applications due to its excellent biocompatibility and bioactivity [1]. However, mechanical properties of HA are insufficient for major load-bearing applications. Deposition of HA coatings onto metallic substrates such as Ti and Ti-alloys is therefore carried out to overcome such issues [2]. It was reported that bioactive HA coatings on metallic implants could

(1) promote earlier stabilization of the implants in the surrounding bone, (2) support bone in-growth and improve the implant-bone bonding strength, (3) decrease the release of metallic ions from the implants, thereby reducing possible toxicity in the vascular system and subsequent health hazards, and (4) shield the prosthesis implants from environmental attacks to facilitate long-term function performance, therefore lowering the risk of their failure and extend their functional life [3, 4]. However, when implanted in vivo, the repetitive loading and rubbing contact with counter materials or surrounding tissue experienced by the coatings can result in easy removal of materials and release of debris particles, thereby jeopardizing the mechanical and biological performance, which in turn may lead to an early failure of the whole structure in service. Therefore, investigation into the tribological behavior of HA coatings has emerged as an important issue in both the research filed and clinical applications [5, 6]. In order to improve the wear resistance and other properties of HA coatings, it is of special importance to optimize the fabrication process used for HA coating deposition [4].

Plasma spray processes have been widely used for various industrial applications due to their versatility, high deposition rates and a wide range of applicable materials [4]. Although the processes are presently used to deposit protective and biocompatible HA coatings on Ti and Ti-alloy substrates, numerous issues such as insufficient coating adhesion, coating fractures, and thermal shock to the substrate materials are still reported [4, 7]. The issues have been addressed individually by focusing on various aspects of the plasma spray process [7]. One of such aspects is the in-flight properties (such as temperature and velocity) that the sprayed material particles attain within the plasma jet. It has been shown that such factors significantly influence the structure, density, and the coating-substrate bonding strength [4, 8-10].

The previous studies of plasma sprayed HA coatings have aimed at physical, mechanical and chemical properties [4, 8, 11]. Tribological properties of such HA coatings deposited on metallic substrates have been less reported. Fu et al. [12] investigated fretting wear of thermally sprayed HA coatings under dry conditions and found that the HA coatings had poor resistance to

wear. Dey and co-workers [5] developed microplasma sprayed HA coatings with poor scratch and wear resistance.

Hanks' solution has physiological pH and salt concentration and is thus widely used in cell culture as a buffer system. It can further be used to simulate body fluid conditions to study the bio-tribological properties of thermally sprayed coatings under physiological conditions. Although the morphological and structural changes associated with dissolution of plasma sprayed HA coating in Hanks' solution have been studied widely, the effect of Hanks' solution (or other physiological media) on the tribological behavior of HA coatings has been much less studied [13-16].

In this study, four different HA coatings were deposited onto commercially available Ti6Al4V substrates via plasma spray process by systematically varying the in-flight particle velocities. The coatings tribological properties with and without Hanks' solution were systematically investigated using ball-on-disc micro-tribological test.

2. Experimental details

2.1. Sample preparation

In-house fabricated spray-dried HA powders with diameters of 39.9 ± 10.6 μm were used as the feedstock. The details of the HA powder preparation were reported in the previous studies [4, 8]. For the substrates, commercially available Ti6Al4V alloy (99.9% purity, Titan Engineering, Singapore) were cut to 10 mm × 10 mm × 2 mm coupons. Atmospheric plasma system (Praxair Inc., Danbury, USA) equipped with SG-100 gun was employed to deposit the HA coatings. Purified argon was used as the main arc forming gas and carrier gas, while helium was used as an auxiliary enthalpy gas. In total, four runs with different system parameters were carried out to produce coatings under different in-flight properties (from [8]). Annotation of the four samples (HA1 to HA4) is provided in Table 1 along with the corresponding values of the system parameters. The selection of the process parameters was based on prior work reported in [4, 16]. During the spraying, the in-flight particle properties (temperature and velocity) were measured with

a fast-shutter CCD laser-assisted camera (Oseir Ltd., Tampere, Finland). The measured values are further provided in Table 1.

2.2. Characterization

The surface morphology and topography of the coatings were studied using SEM (JEOL-JSM-5600LV, Japan) and surface profilometry (Talyscan 150 with 4 μm diameter diamond stylus, Taylor Hobson, UK). Three measurements per sample were carried out to obtain average root-mean-squared surface roughness (R_q). To evaluate the coatings microstructure, sample cross-sections were ground using 800, 1200, 2400 and 4000 grit SiC papers and polished to 1 μm surface finish with diamond paste. The phase composition of the coatings was examined using X-ray diffractometer (Philips MPD 1880, PANalytical, the Netherlands) with Cu K_α radiation at 40 kV and 30 mA and the chemical composition was studied using energy-dispersive X-ray spectroscopy (EDX, Model 6647, Oxford Instruments, UK).

Nanoindentation has been proved to be a powerful method to measure the mechanical properties of thermally sprayed ceramic coatings, and has the capability to probe individual splats inside the coating [17]. Young's modulus (E) and hardness (H) were measured by nanoindentation (Agilent G200, Keysight Technologies, USA) on the polished cross section of the coatings. The continuous stiffness measurement technique was used, with the strain rate target and depth limit being 0.05 s^{-1} and 2000 nm, respectively. In total 20 indentations were made on each sample to obtain the average E and H values. The tribological properties of the samples were investigated using ball-on-disc micro-tribological test (CSM High Temperature Tribometer, CSM Instruments SA, Switzerland) against 100Cr6 steel balls (R_q = 0.032 μm, H = 7.5 GPa) of 6 mm in diameter in a circular path of 1 mm in radius for 40000 laps at a sliding speed of 2 cm/s under a normal load of 3 N at room temperature (22-24°C). In order to eliminate the influence of the substrate during the subsequent tribological testing, the coatings were deposited so that the thickness exceeded 300 μm [18]. The samples were tested in both air and Hanks' solution (H9269, Sigma-Aldrich, Singapore).

Three measurements per sample were carried out to obtain the average friction coefficient. Considering the difficulty in measuring the wear depth due to the relatively high surface roughness of the coatings, the wear width was used as the major index to assess the wear resistance of the different HA coatings in this study. The width of the wear tracks was measured by surface profilometry. Wear morphology of the steel balls rubbed against the HA coatings under dry conditions was observed by light microscopy (Zeiss Axioskop 2 with JVC Color Video Camera, Carl Zeiss, Germany). Due to extensive corrosion, the wear morphology of the steel balls tested under wet conditions is not included in the paper due to low information yield.

3. Results and discussion

3.1. Coating properties

As determined by Rietveld analysis of the obtained XRD spectra, the dominant phase in the produced powder is HA [4, 19]. A 5% $CaCO_3$ content was detected; this could have originated in the material by a reaction of the original $Ca(OH)_2$ with atmospheric CO_2 during the powder production [4]. After the plasma spray process, the produced coatings mainly consisted of HA, with varying content of metastable tri-calcium and tetra-calcium phosphate phases (α-TCP, β-TCP, TTCP), as reported earlier in [4].

The surface topography of the as-sprayed HA coatings is presented in Fig. 1 and Fig. 2. The R_q values of the as-sprayed coatings are summarized in Table 2. It was found that the HA1 coatings exhibited a relatively rough surface topography with a number of protruded particles above the surface, yielding the highest R_q value. The existence of such particles can probably be attributed to the small degree of deformation of the HA particles at a low in-flight velocity, as can be observed in Fig. 2. The HA2 coatings exhibited smaller R_q due to a significantly smaller number of the protruded particles (Fig. 1). Presumably, the decline in the protrusions quantity was triggered by the higher impact energy of the HA particles via increasing the in-flight particle velocity (to ~204 m/s). This was confirmed via SEM as increased HA particles flattening was observed in the

HA2 coatings (Fig. 2). No large protruded particles could be seen in the surface topography (Fig. 1) images of the HA3 and HA4 coatings, leading to a further decrease in the R_q values. The HA4 coating exhibited the smoothest surface topography and lowest R_q value probably due to the highest compaction of the surface via the highest in-flight particle velocity (275 m/s).

Fig. 3 presents the cross-sectional morphology and microstructure of the HA coatings. The highest number of inter-particle gaps was found in the HA1 coating, probably due to the weak inter-particle bonding in the coating as it was deposited at the lowest in-flight particle velocity [5, 12]. Additionally, compared with the other three coatings, HA1 coating showed the smallest amount of particle deformation, with some HA particles still retaining their spherical shape. As the in-flight particle velocity increased in HA2-4, the inter-particle gaps were significantly reduced (Fig. 3), implying stronger inter-particle bonding in those coatings. While large pores (~50 μm or above) could be observed in the HA2 coating, they were absent on the cross-section of the HA3 and HA4 coatings. This further proves that higher in-flight particle velocity resulted in denser microstructure of the coatings. The results signify that the in-flight particle velocity is an important factor in controlling the microstructure, and thereby possibly influencing the wear resistance of the plasma sprayed HA coatings.

It can be seen in Fig. 4 that the E and H of the coatings generally increased with the in-flight particle velocity. The respective values of HA4 (E = 77.3 GPa, H = 4.9 GPa) are highest among the four coatings and represent a 26.9 % and 37.3 % improvement, respectively, as compared with HA1. Such increase is probably associated with the lowest porosity (i.e., the most compact structure) obtained under the highest in-flight particle velocity during the plasma spray process. In addition, the inter-particle bonding, which is believed to be strengthened at higher in-flight particle velocities, can affect the sample displacement during nanoindentation. This in turn would influence the obtained E and H values [20]. Nanoindentation has been extensively used to investigate the mechanical properties of HA coatings. Saber-Samandari et al. [17] reported that the E and H of flame sprayed HA coatings to be in the range of 114-121 GPa and 5.0-5.8 GPa, respectively. In the

study of Surmeneva et al [21], the E and H values of RF magnetron sputter-deposited HA coating were reported to be 112 GPa and 7.0 GPa, respectively. Both studies therefore obtained coatings with higher E and H than in the presented study. On the other hand, some other studies reported much lower E and H values. For instance, McManamon et al. [22] found that their plasma sprayed HA coatings possessed a E of 4.1 GPa and a H of 0.29 GPa; low E (6 GPa) and H (1 GPa) were also obtained by Sidane et al. [23] for their sol-gel HA coating, although they used the same indentation depth and strain rate as our study. These results suggest that the mechanical properties of HA coatings depend on various factors such as crystallinity, porosity, particle size and processing routes. It should be pointed out that overall the E and H values obtained here agree well with those reported in a number of previous studies on pure HA ceramics [24, 25].

It is worth mentioning that HA1 showed significantly higher variation in E and H (error bar in Fig. 4) than the other coatings. Fabricated under the lowest in-flight particle velocity, HA1 possessed the least compact microstructure and its highest porosity and inhomogeneous pore distribution probably induced the measured data scatter.

3.2. Tribological properties

Fig. 5a presents the mean friction coefficients of the four different HA coatings tested against a 100Cr6 steel ball without and with Hanks' solution. The friction coefficients of the HA coatings presented in Fig. 5a were averaged from the global trends of friction coefficient versus laps presented in Fig. 5b. The measured friction coefficients well correlate to the respective in-flight velocities (Table 1): the increased in-flight particle velocity significantly decreased the friction of the HA coatings probably through the decreased roughness of the surfaces. At the same time, an improved wear resistance of the HA coatings was observed. In addition, all the HA coatings tested with Hanks' solution exhibited lower friction coefficients as opposed to their counterparts tested under dry conditions. The reason is that the Hanks' solution lubricated the rubbing surfaces and prevented a direct solid-solid contact between them during the sliding [26-28].

Fig. 5b illustrates the development of the HA coatings friction coefficients tested without and with Hanks' solution as a function of the number of laps. The HA coatings deposited at the higher in-flight particle velocities exhibited lower friction during the entire sliding without and with Hanks' solution as a result of a lower wear of the coatings. Under the wet conditions, the HA coatings generally showed lower friction coefficients with respect to laps due to the lubricating effect of the solution [26].

The high surface roughness of the HA coatings lessened their contact areas with the counter steel balls under the dry condition, therefore the corresponding initial friction coefficients of the coatings were relatively low (Fig. 5b). Subsequently, the increased wear of the rubbing surfaces with increased laps in the running-in period increased the contact area between them, yielding the increased friction of the HA coatings. The HA coatings tested with Hanks' solution did not exhibit the relatively low friction in the beginning phase as the presence of the solution between two rubbing surfaces mitigated the influence of surface roughness on the initial friction of the coatings. During the prolonged sliding, the lower surface roughness of the HA coatings gave rise to their lower friction because of the reduced mechanical interaction between asperities of the two rubbing surfaces under both dry and wet conditions.

Fig. 6 shows the wear widths of the different HA coatings tested with and without Hanks' solution. It was found that the widths of the wear tracks of the HA coatings tested under both conditions significantly decreased at higher in-flight particle velocities through the enhanced inter-particle bonding, and increased E and H of the fabricated coatings. In addition, the HA coatings tested with Hanks' solution exhibited lower wear (i.e., narrower wear tracks) as opposed to their dry-tested counterparts, confirming the lubricating effect of the Hanks' solution. The similar trends between the friction (Fig. 5a) and wear (Fig. 6) of the HA coatings imply that the frictional behavior of the HA coatings is closely related to their wear behavior.

After the tribological tests, the wear topography and morphology of the HA coatings were examined. As shown in Fig. 7, the dry sliding of the steel ball against the HA1 coating removed the

surface material up to a wear depth of 46 ± 5 μm. The introduction of the Hanks' solution during the sliding led to a decrease in the wear depth of the HA1 coating to 28 ± 3 μm (Fig. 7).

Fig. 8 shows the wear morphology of the HA coatings tested without Hanks' solution. It was consistently found that the HA1 coating exhibited significant material removal during the dry sliding against the steel ball. Such material removal was not observed for the other HA coatings tested under the dry conditions (Fig. 8) due to their higher abrasive wear resistance. The wear track width (indicated by arrows in Fig. 8) of the HA coatings significantly decreased with increasing particle velocity. Following this trend, the HA4 coating tested under dry conditions did not exhibit a significant wear track on the surface. The results therefore confirmed the assumption that the increased in-flight particle velocity greatly improves the abrasive wear resistance of the HA coatings under the dry conditions.

Fig. 9 shows the wear morphology of the HA coatings tested with Hanks' solution. The introduction of Hanks' solution during the sliding against the steel ball significantly reduced the abrasive wear of the HA1 coating, as confirmed by its smaller wear width and depth (Fig. 7). In addition, the presence of Hanks' solution between two rubbing surfaces can lessen the adhesive wear of the HA coatings by serving as a spacer to prevent a direct content between the rubbing surfaces. Similar to the dry condition, it was found that the wear track width (indicated by arrows in Fig. 9) of the HA coatings tested with Hanks' solution decreased according to the relation of HA1 > HA2 > HA3 > HA4 due to the increased abrasive wear resistance of the HA coatings associated with higher in-flight particle velocities. Overall, the SEM observation clearly showed that the HA coatings exhibited a decrease in their friction and wear with the increased in-flight particle velocity under both dry and wet sliding conditions and the introduction of Hanks' solution during the sliding apparently lowered the friction and wear of all HA coatings most likely due to the lubricating effect of the Hanks' solution.

The EDX measurement within the wear track of the HA4 coating tested with Hanks' solution detected C, Ca, O, and P presence. The Ca, O, and P peaks are associated with the HA

matrix and the C peak could probably be attributed to surface carbon contamination. No Fe associated with the wear of the steel ball was detected in the spectra, suggesting that no significant (detectable) transfer of Fe into the HA coating occurred.

The effect of the surface roughness on the tribological properties of the HA coatings must be further taken into account. A rougher surface can lead to a higher friction and wear via increased mechanical interaction between the two rubbing surfaces [29-32]. As shown in Table 2, a strong correlation between the surface roughness and friction and wear properties of the HA coatings was observed, thereby clearly indicating that the surface roughness of the HA coatings has a significant influence on their friction in terms of mechanical interaction.

The surface roughness, friction coefficient and wear width values vs. in-flight particle velocity normalized to those of HA1 are presented in Fig. 10a. Marked decreasing trends were detected for all the parameters, indicating that a higher in-flight particle velocity resulted in smoother HA coatings with enhanced friction and wear resistance. Furthermore, when these parameters were normalized to the corresponding values of HA1 and plotted against the surface roughness (Fig. 10b), similar decreasing trends were observed, implying a strong correlation between the friction and wear properties and the surface roughness of the coatings. It is suggested here that the reduction of the wear widths by increasing in-flight particle velocity was realized through a smoother surface topography, i.e. less mechanical interaction between the rubbing surfaces. In addition, when smoother coating surfaces were obtained under higher in-flight particle velocities, Hanks' solution was able to prevent a direct solid-solid contact between two smooth surfaces more effectively, thereby further reducing the friction coefficient.

Fig. 11a and b shows the rubbing surface morphology of the 100Cr6 steel balls used for the HA1 and HA4 coatings after dry wear tests, respectively. The steel ball rubbed on the HA4 coating had a significantly larger wear width of 658 ± 86 μm than the one of the HA1 coating (wear width of 236 ± 54 μm). Such result further supported the idea that the HA4 coating deposited at the

higher in-flight particle velocity possessed a higher wear resistance, giving rise to the higher wear of its counter steel ball during the prolonged sliding [26].

4. Conclusions

Hydroxyapatite coatings were deposited onto Ti6Al4V substrates via atmospheric plasma spray process by systematically varying the in-flight powder particle velocities. The tribological properties of the coatings without and with Hanks' solution were investigated using ball-on-disc micro-tribological test. The SEM observation showed that the HA coatings deposited at higher in-flight particle velocities exhibited smoother surface topography and improved Young's modulus and hardness. As a result, the corresponding HA coatings exhibited significantly lower friction coefficients and wear against the steel ball under both dry and lubricated (Hanks' solution) conditions. The HA coatings tested with Hanks' solution had lower friction and wear due to the boundary lubricant effect of the solution. It is therefore concluded that higher in-flight particle velocity enhances the tribological properties of the HA coatings under both dry and wet conditions.

Acknowledgments

The work of Jan Cizek has been supported by the project NETME Centre Plus (Lo1202), project of Ministry of Education, Youth and Sports under the "National Sustainability Programme". Support of Czech Science Foundation project Nr. 13-35890S and FME BUT specific research project FSI-S-14-2427 is further acknowledged.

References

[1] Hench LL. Bioceramics: from concept to clinic. J Am Ceram Soc 1991:1487-510.

[2] Gross KA, Gross V, Berndt CC. Thermal analysis of amorphous phases in hydroxyapatite coatings. J Am Ceram Soc 1998:106-12.

[3] Lacefield WR. Hydroxyapatite Coating, in An Introduction to Bioceramics. In: Hench LL, Wilson J, editors. Advanced Series in Ceramics: World Scientific Publishing Co. Pte. Ltd.; 1993. p. 223-38.

[4] Cizek J, Khor KA. Role of in-flight temperature and velocity of powder particles on plasma sprayed hydroxyapatite coating characteristics. Surface and coatings technology 2012:2181-91.

[5] Dey A, Sinha A, Banerjee K, Mukhopadhyay AK. Tribological studies of microplasma sprayed hydroxyapatite coating at low load. Materials Technology: Advanced Biomaterials 2014:B35-B40.

[6] Liu Y, Dang Z, Wang Y, Huang J, Li H. Hydroxyapatite/graphene-nanosheet composite coatings deposited by vacuum cold spraying for biomedical applications: Inherited nanostructures and enhanced properties. Carbon 2014:250-9.

[7] Khor KA, Gu YW, Quek CH, Cheang P. Plasma spraying of functionally graded hydroxyapatite/Ti–6Al–4V coatings. Surface and Coatings Technology 2003:195-201.

[8] Cizek J, Khor KA, Prochazka Z. Influence of spraying conditions on thermal and velocity properties of plasma sprayed hydroxyapatite. Materials Science and Engineering: C 2007:340-4.

[9] Cizek J, Khor KA, Dlouhy I. In-Flight Temperature and Velocity of Powder Particles of Plasma-Sprayed TiO2. J Therm Spray Technol 2013:1320-7.

[10] Cizek J, Dlouhy I, Siska F, Khor KA. Modification of Plasma-sprayed TiO2 Coatings Characteristics via Controlling the In-flight Temperature and Velocity of the Powder Particles. Journal of Thermal Spray Technology 2014:1339-49.

[11] Vahabzadeh S, Roy M, Bandyopadhyay A, Bose S. Phase stability and biological property evaluation of plasma sprayed hydroxyapatite coatings for orthopedic and dental applications. Acta Biomaterialia 2015:47-55.

[12] Fu YQ, Batchelor AW, Wang Y, Khor KA. Fretting wear behaviors of thermal sprayed hydroxyapatite (HA) coating under unlubricated conditions. Wear 1998:132-9.

[13] Reis RL, Monteiro FJ. Crystallinity and structural changes in HA plasma-sprayed coatings induced by cyclic loading in physiological media. Journal of Materials Science: Materials in Medicine 1996:407-11.

[14] Whitehead RY, Lucas LC, Lacefield WR. The effect of dissolution on plasma sprayed hydroxylapatite coatings on titanium. Clinical materials 1993:31-9.

[15] Lin JH, Liu ML, Ju CP. Morphologic variation in plasma‐sprayed hydroxyapatite‐bioactive glass composite coatings in Hank's solution. Journal of biomedical materials research 1994:723-30.

[16] Fu YQ, Batchelor AW, Khor KA. Fretting wear behavior of thermal sprayed hydroxyapatite coating lubricated with bovine albumin. Wear 1999:98-102.

[17] Saber-Samandari S, Gross KA. Nanoindentation on the surface of thermally sprayed coatings. Surf Coat Technol 2009:3516-20.

[18] Cizek J. Thermally sprayed bio-ceramic coatings: a study on process parameters influence on coating properties [PhD theis]: Nanyang Technological University; 2010.

[19] Young RA. The Rietveld method. IUC monographs on crystallography 5, International Union of Crystallography: Oxford University Press; 1993.

[20] Oliver WC, Pharr GM. Measurement of hardness and elastic modulus by instrumented indentation: Advances in understanding and refinements to methodology. J Mater Res 2004:3-20.

[21] Surmeneva MA, Mukhametkaliyev TM, Tyurin AI, Teresov AD, Koval NN, Pirozhkova TS, et al. Effect of silicate doping on the structure and mechanical properties of thin nanostructured RF magnetron sputter-deposited hydroxyapatite films. Surf Coat Technol 2015:176-84.

[22] McManamon C, de Silva JP, Power J, Ramirez-Garcia S, Morris MA, Cross GLW. Interfacial Characteristics and Determination of Cohesive and Adhesive Strength of Plasma-Coated Hydroxyapatite via Nanoindentation and Microscratch Techniques. Langmuir 2014:11412-20.

[23] Sidane D, Chicot D, Yala S, Ziani S, Khireddine H, Iost A, et al. Study of the mechanical behavior and corrosion resistance of hydroxyapatite sol–gel thin coatings on 316 L stainless steel pre-coated with titania film. Thin Solid Films 2015:71-80.

[24] Gross KA, Saber-Samandari S. Revealing mechanical properties of a suspension plasma sprayed coating with nanoindentation. Surf Coat Technol 2009:2995-9.

[25] Song J, Liu Y, Zhang Y, Jiao L. Mechanical properties of hydroxyapatite ceramics sintered from powders with different morphologies. Materials Science and Engineering: A 2011:5421-7.

[26] Khun NW, Frankel GS, Sumption M. Effects of Normal Load, Sliding Speed, and Surface Roughness on Tribological Properties of Niobium under Dry and Wet Conditions. Tribology Transactions 2014:944-54.

[27] Wong HC, Umehara N, Kato K. Frictional characteristics of ceramics under water‐lubricated conditions. Tribology Letters 1998:303-8.

[28] Khun NW, Liu E. Tribological behavior of polyurethane immersed in acidic solution. Tribology Transactions 2012:401-8.

[29] Svahn F, Kassman-Rudolphi Å, Wallen E. The influence of surface roughness on friction and wear of machine element coatings. Wear 2003:1092-8.

[30] Menezes PL, Kailas SV. Influence of surface texture and roughness parameters on friction and transfer layer formation during sliding of aluminium pin on steel plate. Wear 2009:1534-49.

[31] Barrett TS, Stachowiak GW, Batchelor AW. Effect of roughness and sliding speed on the wear and friction of ultra-high molecular weight polyethylene. Wear 1992:331-50.

[32] Khun NW, Zhang H, Yang J, Liu E. Mechanical and tribological properties of epoxy matrix composites modified with microencapsulated mixture of wax lubricant and multi-walled carbon nanotubes. Friction 2013:341-9.

Table caption

Table 1: Plasma spray process parameters used for deposition of different HA coatings

Table 2: Surface roughness (R_q) and wear properties of different HA coatings

Figure captions

Fig. 1: Surface topography of as-sprayed HA coatings.

Fig. 2: Surface morphology of as-sprayed HA coatings.

Fig. 3: Microstructure of as-sprayed HA coatings.

Fig. 4: Young's modulus and hardness of as-sprayed HA coatings.

Fig. 5: (a) Friction coefficients of HA coatings tested with and without Hanks' solution; (b) friction coefficients of HA coatings as a function of the number of laps.

Fig. 6: Wear track widths of different HA coatings.

Fig. 7: Surface topography of HA1 coatings after tribological testing without and with Hanks' solution.

Fig. 8: Wear morphology of HA coatings observed after tribological testing without Hanks' solution. Arrows indicate wear widths.

Fig. 9: Wear morphology of HA coatings observed after tribological testing with Hanks' solution. Arrows indicate wear widths.

Fig. 10: Surface roughness, friction coefficient and wear width of HA coatings normalized to the corresponding values of HA1 vs. (a) in-flight particle velocity and (b) surface roughness.

Fig. 11: Wear morphology of 100Cr6 steel balls rubbed on (a) HA1 and (b) HA4 coatings under dry sliding conditions.

Table 1

Set annotation	Net power [kW]	Main gas [L/min]	Auxiliary gas [L/min]	Feed rate [rpm]	Carrier gas [L/min]	Spray distance [mm]	Temperature [K]	Velocity [m/s]
HA1	7	20	10	2	3	75	2540	175
HA2	7	34	24	3	5	100	2513	204
HA3	11	48	38	2	3	100	2500	243
HA4	11	34	24	4	7	75	2470	275

Table 2

Sample	R_q [µm]	Friction coefficient		Wear width [µm]	
		Without Hanks' solution	With Hanks' solution	Without Hanks' solution	With Hanks' solution
HA1	18.7 ± 1.4	0.79 ± 0.03	0.61 ± 0.01	1267.5 ± 105.6	756.3 ± 42.7
HA2	12.6 ± 1.9	0.67 ± 0.02	0.51 ± 0.12	747.8 ± 106.6	576.7 ± 25.1
HA3	11.0 ± 0.1	0.63 ± 0.06	0.44 ± 0.06	583.5 ± 44.5	402.3 ± 29.7
HA4	8.8 ± 0.2	0.61 ± 0.08	0.32 ± 0.06	337.5 ± 44.0	260.7 ± 8.1

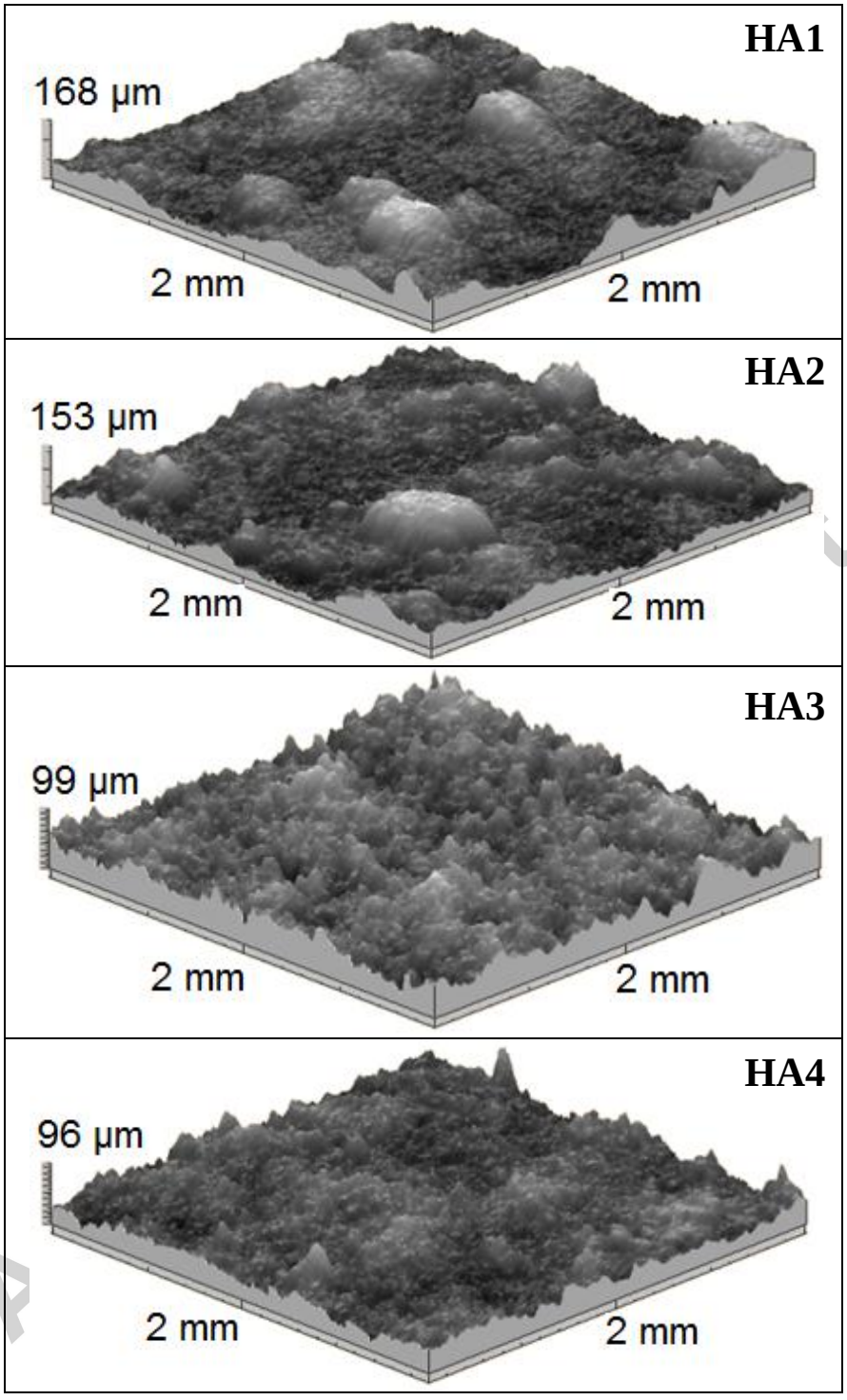
HA1
168 µm
2 mm
2 mm
HA2
153 µm
2 mm
2 mm
HA3
99 µm
2 mm
2 mm
HA4
96 µm
2 mm
2 mm

Fig. 1

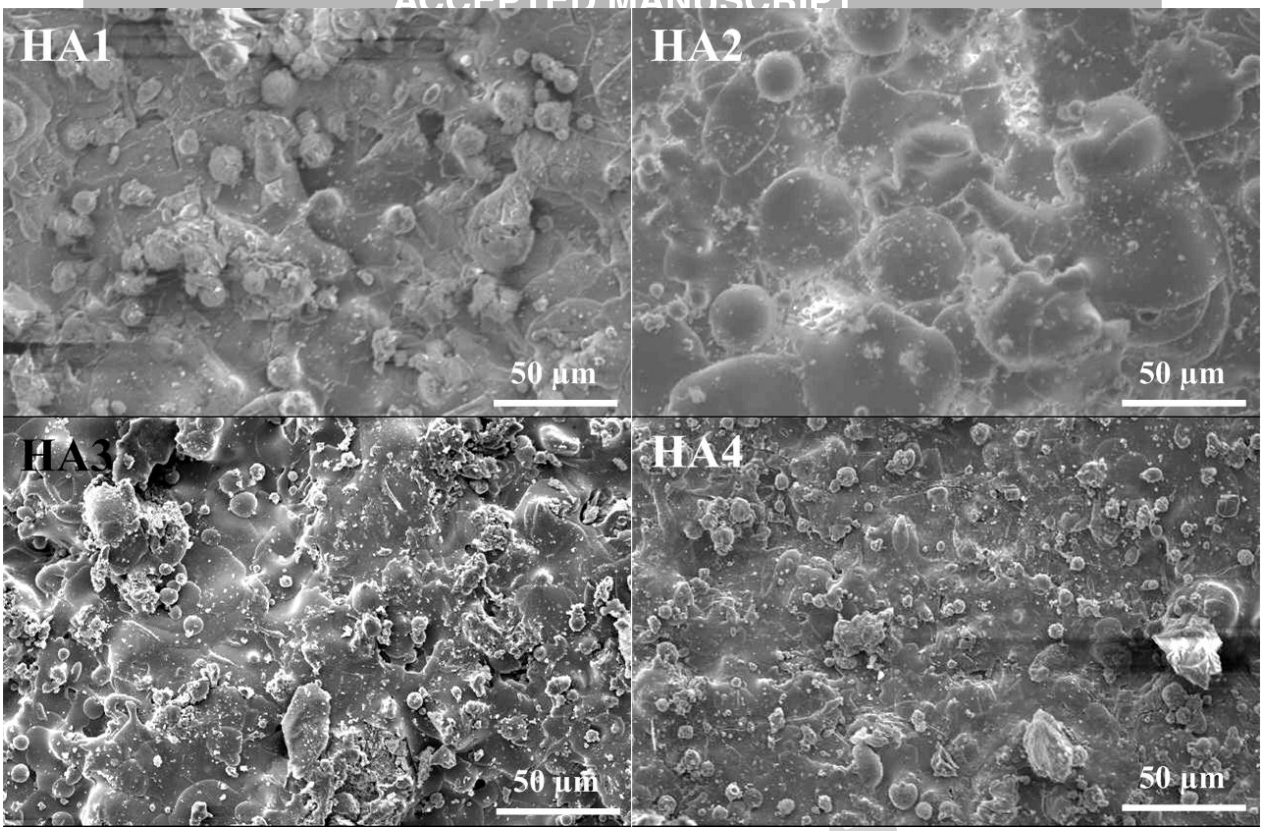

Fig. 2

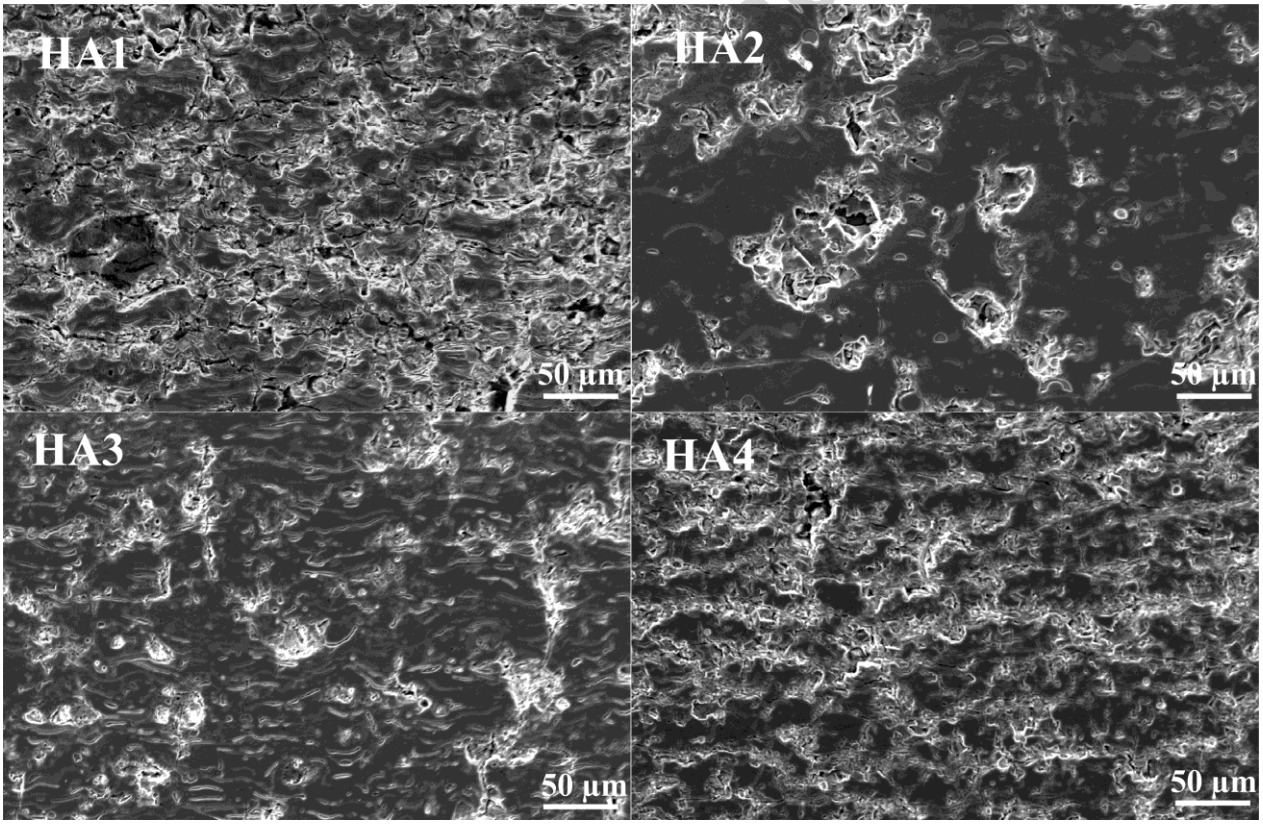

Fig. 3

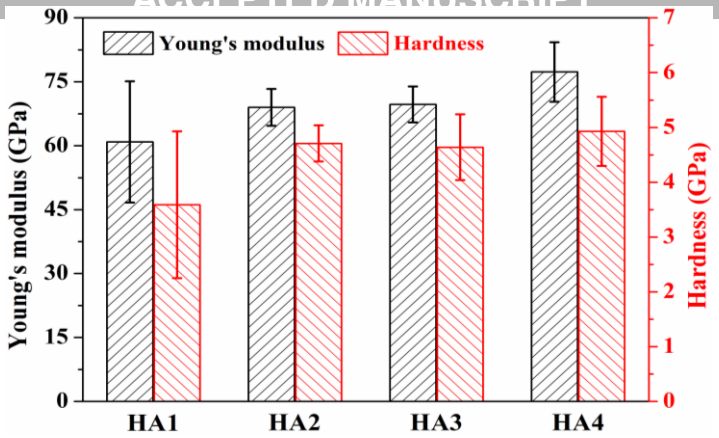

Fig. 4

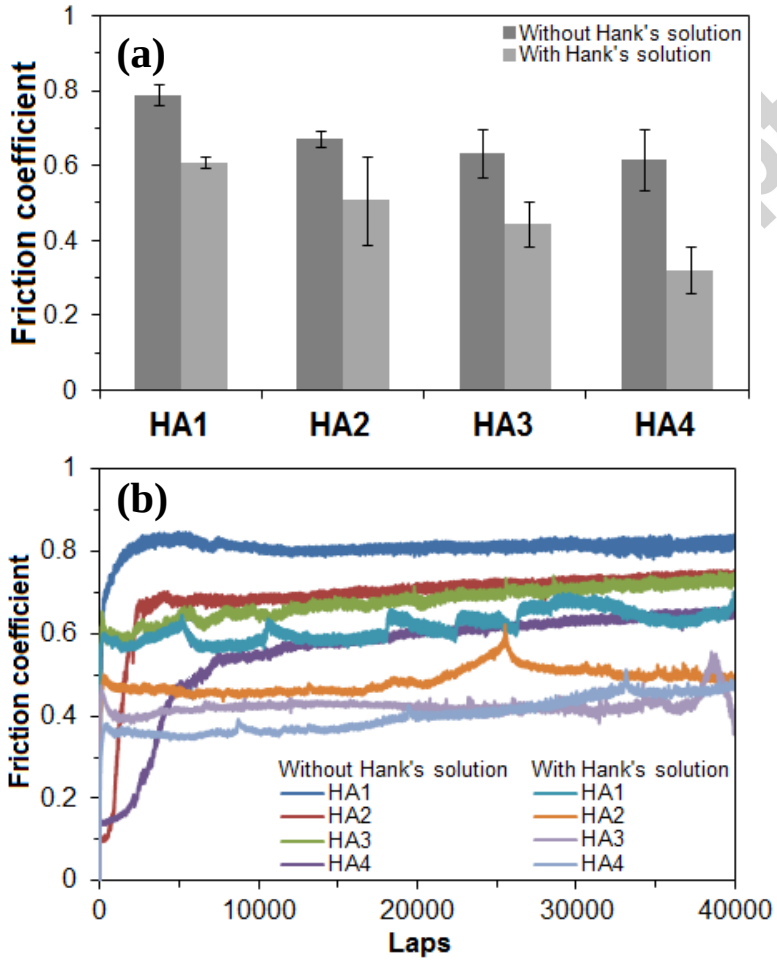

Fig. 5

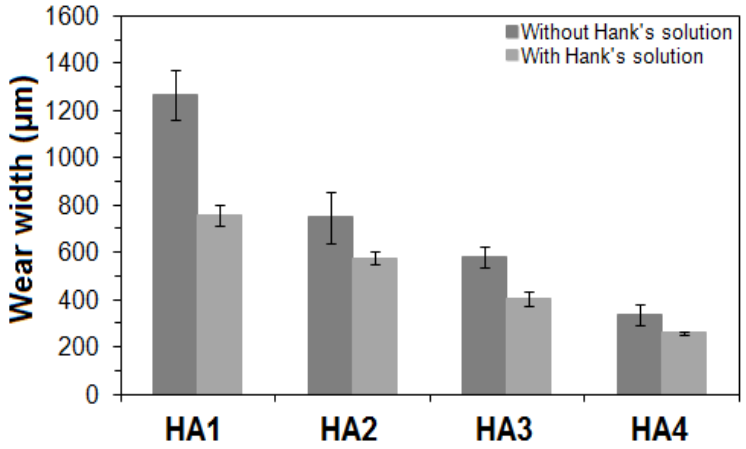

Fig. 6

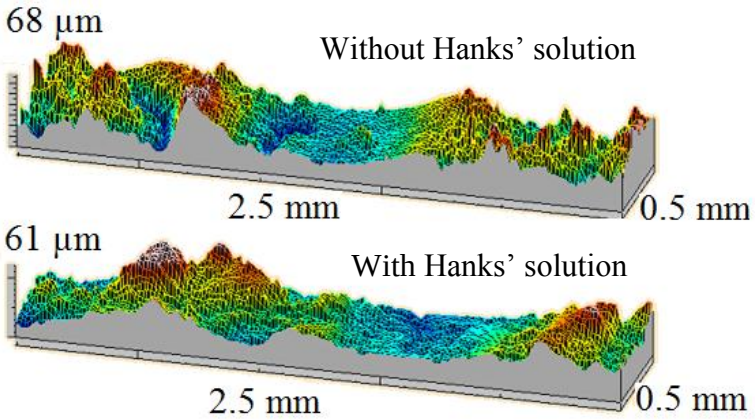

Fig. 7

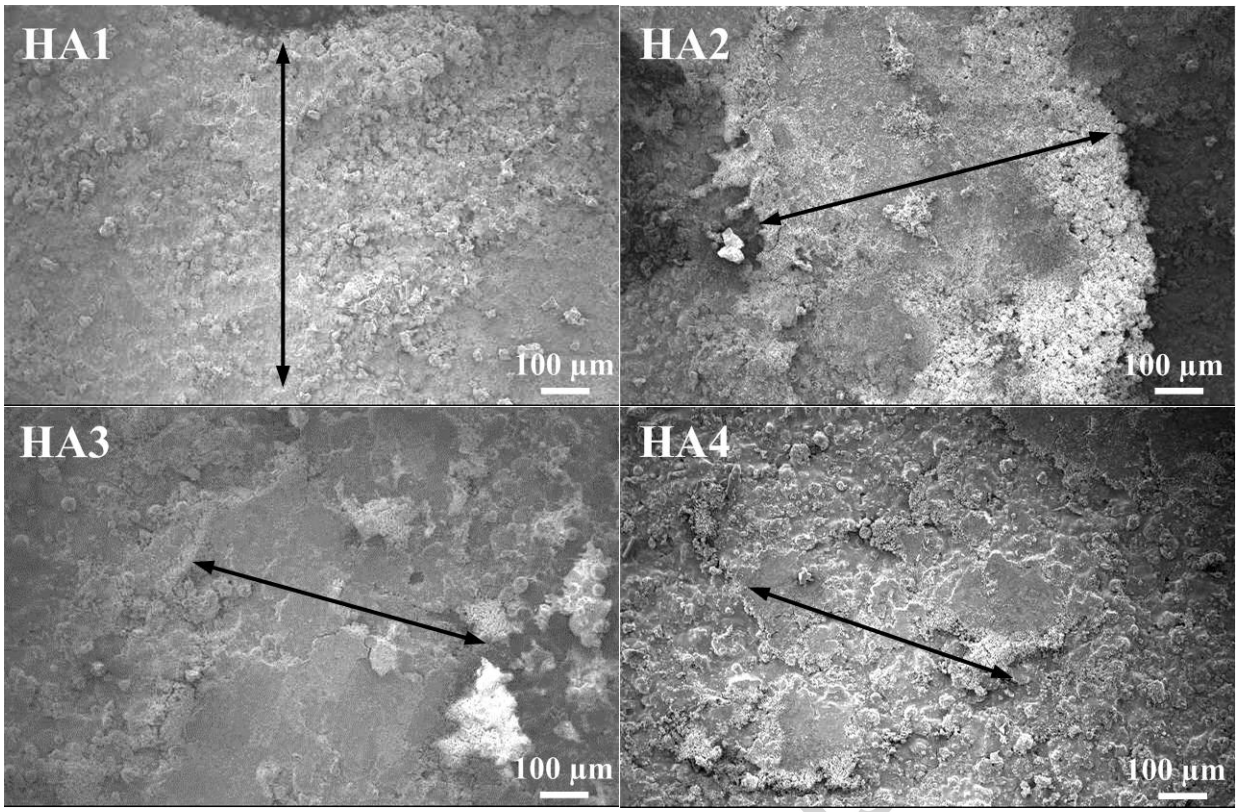
HA1
100 µm
HA2
100 µm
HA3
100 µm
HA4
100 µm

Fig. 8

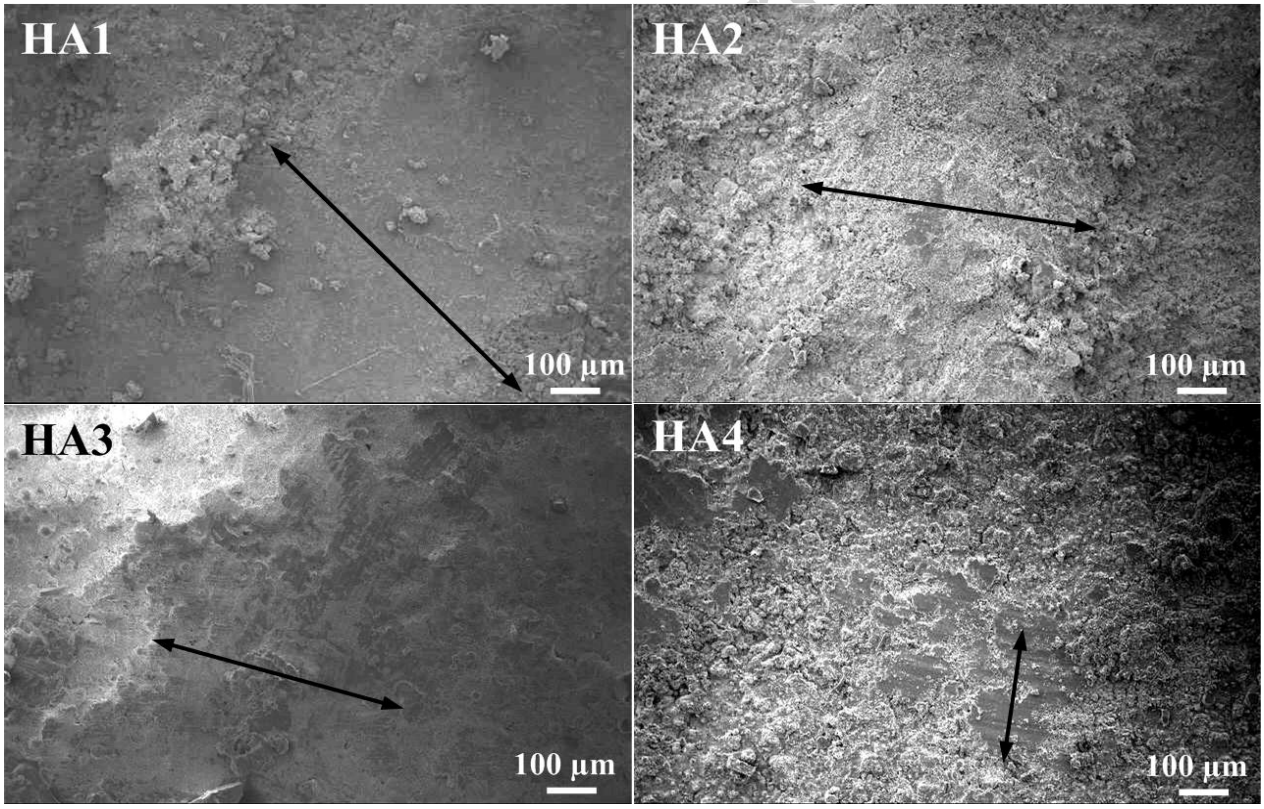
HA1
100 µm
HA2
100 µm
HA3
100 µm
HA4
100 µm

Fig. 9

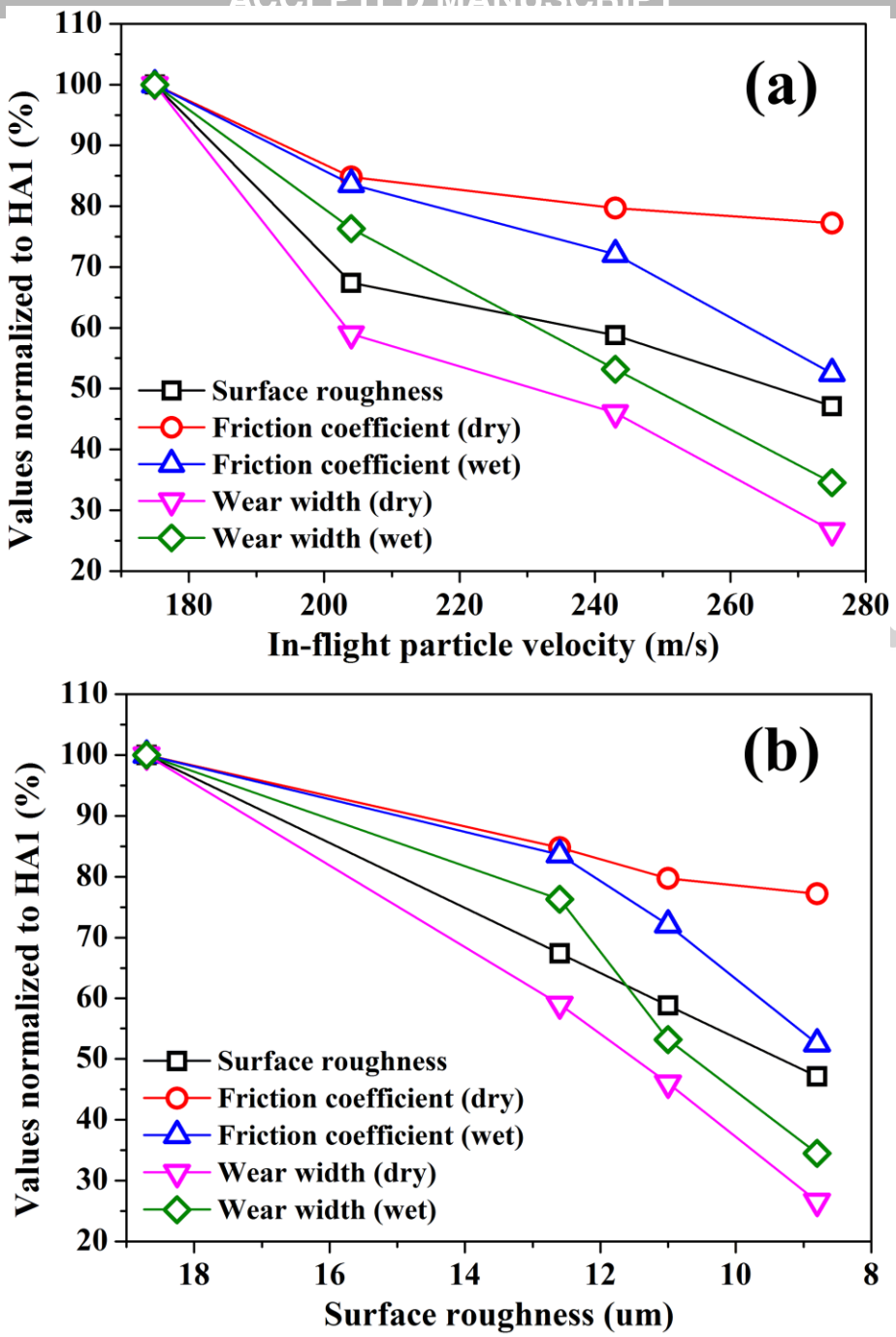

Fig. 10

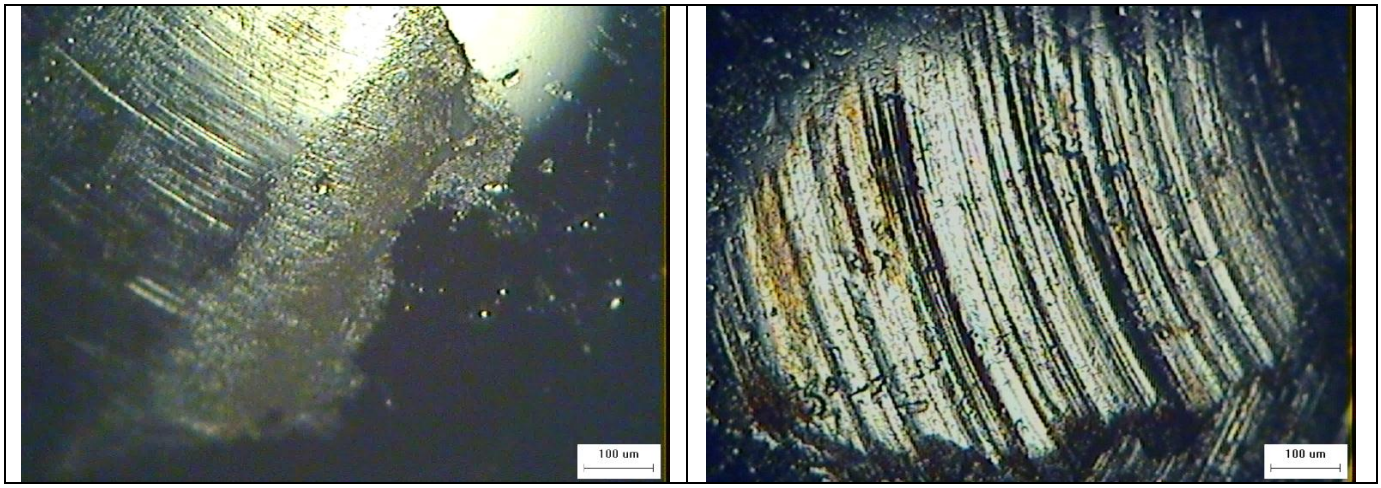

Fig. 11

Highlights

- Higher in-ight velocities resulted in enhanced friction and wear properties of the coatings
- Surface topography and mechanical properties of the coatings were analyzed to understand the underlying mechanisms
- Hanks' solution was used to simulate the in-vitro tribological environment
- The lubrication e_ect of Hanks' solution could reduce friction and wear of the coatings